

Site preference of ternary alloying additions to NiTi: Fe, Pt, Pd, Au, Al, Cu, Zr and Hf

Guillermo Bozzolo^{a,b,*}, Ronald D. Noebe^b and Hugo O. Mosca^c

^aOhio Aerospace Institute, 22800 Cedar Point Rd., Cleveland, OH 44142, USA

^bNASA Glenn Research Center, Cleveland, OH 44135, USA

^cComisión Nacional de Energía Atómica, UAM, Av. Gral. Paz 1499, (B1650KNA) San Martín,
Pcia. de Bs. As. Argentina

Abstract

Atomistic modeling of the site substitution behavior of Pd in NiTi (J. Alloys and Comp. (2004), in press) has been extended to examine the behavior of several other alloying additions, namely, Fe, Pt, Au, Al, Cu, Zr and Hf in this important shape memory alloy. It was found that all elements, to a varying degree, displayed absolute preference for available sites in the deficient sublattice. However, the energetics of the different substitutional schemes, coupled with large scale simulations indicate that the general trend in all cases is for the ternary addition to want to form stronger ordered structures with Ti.

Keywords: Computer Simulations; Nickel; Titanium; Palladium; Platinum, Hafnium, Zirconium, Iron; Aluminum; Copper, Gold; Shape Memory alloy; Semi-empirical methods

1. Introduction

Particular alloying schemes play an important role in controlling or modifying the martensitic transformation temperatures and the structure of the ensuing martensitic phase in NiTi-based alloys. In binary alloys, Ni contents even slightly greater than stoichiometry lead to a rapid decrease in the transformation temperature [1]. For Ti-rich alloys, however, the transformation temperatures are much less sensitive to composition, primarily as a result of the precipitation of Ti₂Ni particles, which leave the composition of the matrix relatively unchanged [2]. Some ternary alloying additions, even at very small levels (for example, Fe or Co substituted for Ni, and Al, Mn, V, or Cr substituted for Ti), will severely depress the transformation temperatures of NiTi alloys but still result in a monoclinic martensite phase after transformation of the matrix. Other

* Corresponding author: NASA Glenn Research Center, M. S. 23-2, Cleveland, OH 44135, USA. Tel: +1-216-4335824; Fax: +1-216-4335170. Guillermo.H.Bozzolo@grc.nasa.gov

alloying additions (for example, Cu in place of Ni [3], or Mn when substituted evenly for Ti and Ni [4]), have relatively little effect on the transformation temperature of NiTi even at large concentrations, but change the martensitic phase from monoclinic to orthorhombic [3]. Then there is a final group of alloying additions, namely Hf, Zr, Au, Pd and Pt, which have been found to increase the transformation temperature of NiTi-based alloys proportional to their concentration, but only in amounts greater than about 10 at%, resulting in an orthorhombic martensite structure below the martensite finish temperature [5].

Knowledge of the site preference behavior of additions to the base alloy is the first step for the understanding of their effect on the shape memory characteristics but, in spite of the relevance of this topic, relatively few experimental [8-11] or theoretical [12,13] studies have been performed to determine the actual site preference of ternary additions to NiTi, the most important of the shape memory alloys due to its superior shape memory behavior and mechanical properties. Recently, however, atomistic modeling has become a helpful aid to alloy development efforts through their ability to determine the site preference of alloying additions and the overall energetics of new alloy systems in a simple and straightforward fashion. An application of an atomistic modeling technique, the BFS method for alloys [6], to the study of Pd site preference in NiTi [7], indicated that a detailed analysis is needed in order to find full compatibility between modeling predictions and experimental work. Having established the groundwork for how site preference behavior can be studied within the framework of a quantum approximate method such as BFS, we now report on the application of this approach to the case of specific ternary additions (Fe, Pt, Au, Al, Cu, Zr and Hf) to NiTi, elements of technological interest to the development of new high-temperature shape memory alloys.

2. The BFS method for alloys

The BFS method for alloys [6] is based on the concept that the energy of formation of a given atomic configuration is the sum of the individual atomic contributions, $\Delta H = \sum \epsilon_i$. Furthermore, each contribution by atom i , ϵ_i , can be calculated as the sum of two terms: a strain energy, ϵ_i^S , computed in the actual lattice as if every neighbor of the atom i were of the same atomic species i , and a chemical energy, ϵ_i^C , computed as if every neighbor of the atom i were in an equilibrium lattice site of a crystal of species i , but retaining its actual chemical identity.

The computation of ε_i^S , using Equivalent Crystal Theory (ECT) [14], involves three pure element properties for atoms of species i : cohesive energy (E_c), lattice parameter (a) and bulk modulus (B_0). These three parameters for each of the constituent elements, listed in Table 1, are needed in the general derivative structure of the final alloy. Consequently, when studying bcc-based alloys such as the B2-structured NiTi, the elements would need to be parameterized as if they were A2 (bcc). Additional ECT parameters, α and λ [14], can be easily derived from E_c , a and B_0 .

The chemical energy, ε_i^C , accounts for the corresponding change in composition, considered as a defect in an otherwise pure crystal. The chemical ‘defect’ deals with pure and mixed bonds, therefore, two additional perturbative parameters (Δ_{AB} and Δ_{BA} where A, B = Ni, Ti, Fe, Pt, Pd, Au, Al, Cu, Zr, Hf) are needed to describe these interactions. A reference chemical energy, $\varepsilon_i^{C_0}$, is also included to insure a complete decoupling of structural and chemical features. Finally, the strain and chemical energies are linked with a coupling function g_i , which ensures the correct volume dependence of the BFS chemical energy contribution. Therefore, the contribution of atom i to the energy of formation of the system is given by

$$\varepsilon_i = \varepsilon_i^S + g_i(\varepsilon_i^C - \varepsilon_i^{C_0}) \quad (1)$$

All the necessary BFS parameters, listed in Table 1, were calculated using the Linearized-Augmented Plane Wave method (LAPW) [15]. We refer the reader to Ref. 6 for detailed discussions of the BFS method, its definitions, operational equations and their implementation.

3. Application of the BFS method to the study of NiTi+X alloys

A previous application of BFS to NiTi+Pd [7] indicates that a complete understanding of the site preference behavior of an element X in NiTi emerges only from a detailed and varied analysis of the situation. First, we perform an atom-by-atom analysis of the energetics of a single atom X in NiTi. In doing so, we can determine absolute site preference of an element in an ordered structure in its dilute limit, as has been successfully done in previous applications of BFS [16]. Second, we extend this analysis to the case of additional X atoms (or increasing concentration of solute), identifying interactions between elements that are not immediately apparent from the limited case

of a single atom. Third, to confirm the trends established with increasing solute concentration and in order to verify their effect in situations that better resemble realistic conditions including finite temperature, we utilize large scale Monte Carlo simulations. Thus, the combination of analytical (atom-by-atom zero-temperature ‘static’ energy calculations) and numerical (Monte Carlo simulations) methods provides a more complete understanding of the behavior of a ternary element X in NiTi, than any one procedure used in isolation, providing results more in line with experimental expectations.

As in previous work [7], large scale simulations of the formation of different NiTi+X (X = Pd, Pt, Hf, Al, Zr, Fe, Cu, Au) alloys, are performed using Monte Carlo - Metropolis exchange algorithms (MCAS) [6,17], which provide information regarding the thermodynamical ground state of the system, and also with a second type of simulation designed to provide a better connection to actual alloy microstructural evolution. This latter technique, a variant of the traditional Monte Carlo - Metropolis algorithm, although approximate in nature, provides a better modeling framework for diffusion processes, thus leading to final states that are more appropriate for comparison with experiment. Known as the BANN algorithm [17], atoms of different species are allowed to exchange with only nearest-neighbor sites until an equilibrium state is reached at each temperature. In addition, the exchanges are accepted or rejected in terms of a probabilistic factor which depends on the available thermal energy. In this way, it is possible for atoms to “lock” themselves into metastable configurations that may be slightly higher in energy than that found using the MCAS method, which allows pairs of atoms to swap *any* two positions within the computational cell until the lowest energy configuration is found.

The initial state, in both types of simulations, consists of Ni, Ti and X atoms randomly situated in a 1024-atom computational cell. A typical temperature cycle in both MCAS and BANN simulations is a monotonic decrease in temperature, with decreasing step sizes (~ 50 K) at or below room temperature. At each temperature stage, the cell is allowed to equilibrate (i.e., no further changes in the energy of formation after a sufficiently large number of exchanges) followed by optimization of the lattice parameter by means of isotropic expansions or compressions of the rigid bcc lattice, in order to minimize the energy of the cell.

The low temperature MCAS results assume that the system will retain a bcc symmetry and not undergo a martensitic transformation. Experiment shows that this is not correct [1], but due to the character of these diffusionless transformations, no significant changes in site preference behavior

would be expected. The martensite phase would retain the basic order of the parent B2 phase. Therefore, we have included these results primarily to show the ordering tendencies of the B2 phase as a function of temperature.

Throughout this work, we use a simple notation to indicate the different possible substitution schemes. If A and B represent the two simple cubic sublattices of the B2 compound, then X(A) denotes an X atom substituting for an atom A on the A sublattice. If the displaced A atom goes on to occupy a site in the B sublattice (A(B)), the two individual point defects can be connected by denoting them as X(A)A(B)_d. In this case, the subindex *d* distinguishes between the pair of defects (X(A) and A(B)) as being nearest neighbors (NN) (*d* = 1), next-nearest neighbors (NNN) (*d* = 2), or the pair being separated by distances greater than that (either no subindex or *d* = *f*).

4. Results and Discussion

Absolute site preference for a dilute solute within an ordered compound can be extracted from the energetics of the different substitutional schemes available to a single atom. For example, in a Ni(Ti,X) alloy, the X atom can occupy the available site in the Ti sublattice, X(Ti), or occupy a site in the Ni sublattice displacing the Ni atom to a Ti site (X(Ni)Ni(Ti)₁, X(Ni)Ni(Ti)₂ or X(Ni)Ni(Ti)_f). An absolute site preference for a particular alloying addition would be one where the element energetically prefers a Ni or Ti site regardless of how the elemental substitution was made, even if that means the additional creation of an antisite defect in order to accommodate the element on its preferred lattice. For example, absolute preference for a Ni site would mean that when a Ni atom is replaced by an X atom, the defect X(Ni) would be lower in energy than the creation of a defect pair of the type X(Ti)Ti(Ni) *and* when a Ti atom is replaced by an X atom, it will still prefer the Ni site such that the creation of a defect pair X(Ni)Ni(Ti) will be lower in energy than a direct X(Ti) substitution. While an absolute site preference is observed for a number of alloying additions to NiAl [16], none of the elements studied show an absolute preference for a particular sublattice in NiTi. Instead, it is energetically preferable for all the elements studied to reside on whatever sublattice they were intended for, though there are differences in the degree to which this behavior occurred.

These results are summarized in Fig. 1, which illustrates the energy gaps for an atom X in Ni(Ti,X) or (Ni,X)Ti alloys. The energy gaps are defined as the difference in energy (in eV)

between an X(Ti) substitution and the average between $X(\text{Ni})\text{Ni}(\text{Ti})_1$ and $X(\text{Ni})\text{Ni}(\text{Ti})_f$ defects for $\text{Ni}(\text{Ti},\text{X})$ alloys, and the difference in energy between X(Ni) and the average between $X(\text{Ti})\text{Ti}(\text{Ni})_1$ and $X(\text{Ti})\text{Ti}(\text{Ni})_f$ for $(\text{Ni},\text{X})\text{Ti}$ alloys. The table included in Fig. 1 displays the difference in energy between a cell with a given substitution and a pure B2 NiTi cell. At first glance, these results show that all the elements studied prefer Ni sites in $(\text{Ni},\text{X})\text{Ti}$ alloys, as it takes a substantial amount of energy to induce the formation of an antisite defect. Similarly, all elements show preference for Ti sites in $\text{Ni}(\text{Ti},\text{X})$ alloys, but with much smaller energy gaps between X(Ti) and X(Ni)Ni(Ti) states. For Fe in $\text{Ni}(\text{Ti},\text{Fe})$ alloys, this gap is exceedingly small indicating, in principle, that when Fe is substituted for Ti it is nearly equally likely to occupy a site in the Ni or Ti sublattice. But when Fe is substituted for Ni, there is a very strong preference for the Fe atom to remain in the Ni sublattice. Therefore, of the elements studied, Fe is the closest one to exhibiting an absolute preference for the Ni-sublattice. For Pd and Pt in $\text{Ni}(\text{Ti},\text{X})$ alloys, the energy gap is still small, indicating that there is a large probability that Pd and Pt could also reside in either sublattice. The other elements (Au, Al, Cu, Zr and Hf) display an increasingly large energy gap, which translates into an increasing likelihood that these elements could be found exclusively in the Ti sublattice in $\text{Ni}(\text{Ti},\text{X})$ alloys. The opposite trend is observed for $(\text{Ni},\text{X})\text{Ti}$ alloys. Following the same sequence, Fe displays the largest energy gap (favoring Fe(Ni) over Fe(Ti)Ti(Ni) substitutions), and Hf displays an energy gap of nearly the same magnitude as that found for $\text{Ni}(\text{Ti},\text{X})$ alloys. The results shown in Fig. 1 suggest that this set of alloying additions, even though they display overall the same site preference behavior, can be loosely divided into different groups (based on the magnitude of the energy gaps) thus facilitating the discussion of the emerging trends.

While these results establish rather simple and useful guidelines for determining the site preference behavior of ternary additions in NiTi, additional modeling results introduce further information that might prove to be useful when comparing modeling predictions with experiment. A procedure to tackle this problem was already detailed for the case of Pd additions to NiTi [7], where it was found that in spite of the results shown in Fig. 1, other factors could come into play when determining the actual behavior at larger solute concentrations. This is especially true for elements like Fe, Pt and Pd, where the absolute energy gap is small for $\text{Ni}(\text{Ti},\text{X})$ alloys and large for $(\text{Ni},\text{X})\text{Ti}$ alloys.

In our analysis, we will frequently make reference to changes in energy in an atomic cell due to the insertion of a ternary addition X in a $(\text{Ni},\text{X})\text{Ti}$ and $\text{Ni}(\text{Ti},\text{X})$ alloy, and label as energy

‘losses’ or ‘gains’ those changes that raise or lower, respectively, the energy of a given configuration. A representative cluster is shown in Fig. 2. For example, the first entry, $\text{Fe}(\text{Ni}) = -1.2497$ eV, means that the contribution to the total energy of formation of a Fe atom in a Ni site is 1.2497 eV lower (‘gain’) than that of the ‘original’ Ni atom in that site. The next entry, $(8x)\text{Ti}_{\text{NN}} = +1.9768$ eV, means that the 8 Ti NN of the $\text{Fe}(\text{Ni})$ atom combine to raise their contribution (‘loss’) to the total energy of formation by 1.9768 eV with respect to the case where the central Ni site is occupied with a Ni atom. Lastly, the third entry, $(6x)\text{Ni}_{\text{NNN}} = +0.0114$ eV, means that the 6 Ni NNN of the $\text{Fe}(\text{Ni})$ atom combine to raise their contribution to the total energy of formation by 0.0114 eV with respect to the case where the central Ni site is occupied with a Ni atom. As a result, there is a net loss in energy (+0.7385 eV), meaning that the introduction of the Fe atom in the central Ni site results in a cell whose total energy of formation is 0.7385 eV higher (net loss) than a perfect NiTi B2 cell.

To facilitate the discussion, as mentioned above, we group the different ternary additions based on their most salient characteristics within the context of a continuous change of the energy gap, as seen in Fig. 1:

a) Fe: The sequence of decreasing difference between the absolute energy gaps starts with Fe, as seen in Fig. 1, which exhibits a substantially different behavior than the other elements considered in this study. While the large energy gap (10.122 eV) between $\text{Fe}(\text{Ni})$ and $\text{Fe}(\text{Ti})\text{Ti}(\text{Ni})$ configurations indicates preference for Ni sites in $(\text{Ni},\text{Fe})\text{Ti}$ alloys, the exceedingly small gap (0.0232 eV) between $\text{Fe}(\text{Ti})$ and $\text{Fe}(\text{Ni})\text{Ni}(\text{Ti})$ configurations makes nearly no distinction between either sublattice in $\text{Ni}(\text{Ti},\text{Fe})$ alloys. Knowledge of the energy gap alone is not necessarily sufficient to determine the ultimate site preference [7]. Following the guidelines introduced in Ref. 7, additional information on the origin of the energy gap can be obtained by examining the atom-by-atom energetics of this second case, Fe in $\text{Ni}(\text{Ti},\text{Fe})$ alloys. This is shown schematically in Fig. 3 and detailed in Table 2. The ‘direct’ substitution (i.e., $\text{Fe}(\text{Ti})$) is shown on the left side of Fig. 3: (a) relative to the original NiTi cell, the substitution of a Ti atom for a Fe atom raises the energy of the cell by 0.8490 eV. The other case, $\text{Fe}(\text{Ni})\text{Ni}(\text{Ti})$, is shown on the right side of Fig. 3 as a series of idealized steps: (b) first, the substitution of a Ni atom for a Fe atom (which raises the energy by 0.7389 eV), followed by the displaced Ni atom occupying the available Ti site (adding another 0.1325 eV). The proximity between $\text{Fe}(\text{Ni})$ and $\text{Ni}(\text{Ti})$ (from $\text{Fe}(\text{Ni})\text{Ni}(\text{Ti})_f$ to $\text{Fe}(\text{Ni})\text{Ni}(\text{Ti})_1$) lowers the energy a small amount, so that the net increase in energy relative to B2 NiTi due to this

defect is 0.8713 eV. The resulting gap, 0.0232 eV, therefore favors Ti substitutions due to a lower energy cost to the system. It is important to note, however, that the energy cost of Fe(Ni) substitutions is actually lower. It is possible then that Fe(Ni) substitutions will dominate even in cases when the deficient site seems to be preferred.

As Fig. 1 shows, the changes in energy due to the substitution of a single Fe atom result in almost identical net losses (relative to a pure B2 NiTi cell) in both cases (in a Ti or Ni site). The first entry in Table 2 indicates the change in energy relative to a pure NiTi cell when a Fe atom occupies an available Ti site: the contribution of the Fe atom to the energy of formation of the cell is 3.8254 eV higher than the contribution of the original Ti atom in that site. The next entries indicate the change in energy of the neighboring eight Ni atoms (-2.4296 eV) and the six Ti NNN (-0.5466 eV) relative to the case where the central site is occupied by a Ti atom instead of a Fe atom. As a result, there is a net change of 0.8492 eV, which is the total energy cost of performing the Fe(Ti) substitution. Similar results are shown for Fe(Ni) substitutions in (Ni,Fe)Ti alloys.

For larger Fe clusters, however, larger losses are realized for Ti substitutions than for Ni. Table 3 displays the gains (-) or losses (+) in total energy of formation due to the presence of two X atoms in neighboring Ti or Ni sites, following the same convention used in Table 2 (i.e., an energy 'loss' ('gain') is defined as an increase (decrease) in the energy of formation of the computational cell with the substitutional defect relative to the original NiTi cell). Table 4 shows the corresponding results for compact clusters of four atoms. Not surprisingly, the increasing energy benefit arises from the larger number of Ti-Fe bonds created when Fe occupies Ni sites. This, added to the low energy cost of creating antistructure Ni(Ti) atoms, suggests that the preference for Ni sites is more favored the larger the Fe cluster is. Therefore, the relative energy losses or gains, favoring one type of substitution over the other, depend on concentration. Based on the results listed in the previous tables, Table 5 summarizes the trends by displaying the gain (or loss) per Fe atom in each case, as a function of the number of Fe atoms in the NiTi cell.

Results of BANN or MCAS simulations illustrate, for a large scale system, the behavior discussed above, introducing the effect of temperature in the interplay of the different effects leading to the final atomic distribution. These results, for all the ternary additions discussed in this work, are shown in Fig. 4 (for Ni(Ti,X) alloys) and Fig. 5 (for (Ni,X)Ti alloys).

A BANN simulation of a $\text{Ni}_{50}\text{Ti}_{44}\text{Fe}_6$ alloy (Fig. 4.a) shows that all Fe atoms go to Ni sites, with evidence of small FeTi domains. MCAS simulations, which yield the lowest energy state

available, result in a B2 FeTi precipitate in the NiTi matrix. The displaced Ni atoms in Ti planes due to Fe(Ni) substitutions order at low temperatures forming a Ni₃Ti precipitate. On the other hand, a BANN simulation of Ni₄₄Ti₅₀Fe₆ results in a B2 (Ni,Fe)Ti cell, while MCAS results show a TiFe precipitate embedded in the NiTi matrix, as shown in Fig. 5.a.

b) Pt, Pd: The sequence in Fig. 1 continues with Pt and Pd. The study of Pd additions to NiTi in a previous application of BFS to site preference analysis [7], added to the similarities in the pure element parameters and the BFS perturbative parameters in Table 1, makes it interesting to contrast the behavior of these two elements. As shown in Fig. 1, while the absolute numbers are slightly different, both elements display the same general behavior if we just focus on the atom (Pd or Pt) and its immediate environment. They will both reside in Ti sites due to energy gains in the environment for Ni(Ti,X) alloys, and prefer Ni sites in (Ni,X)Ti alloys in spite of the energy losses of the surrounding atoms. There is, however, one major difference between Pt and Pd: while both elements induce total energy gains when occupying Ti sites, Pt also introduces a comparable gain when occupying a Ni site, indicating that the behavior displayed by Pd (i.e., abundant Pd(Ni) substitutions in spite of net Pd(Ti) preference) in Ni(Ti,Pd) alloys, is not shared by Pt, which could then be expected to exhibit a stronger preference for Ni sites.

Introducing a second Pt atom generates similar results. Comparing the results for Pd and Pt in Table 3, it can be seen that the differences between them are more noticeable in this case, leading to comparable gains for Ti or Ni substitutions, further erasing the energy gap that initially favors direct substitutions for Ti atoms (as noted in Fig. 1). This can be explained by the larger role of the energy loss per Pt atom when substituting for Ti atoms and the larger energy gain when substituting for Ni atoms. This trend continues, and is further enhanced, when considering a square patch of four X atoms in Ni or Ti sites. The nearest neighbors of the X atoms can be grouped in three sets of equivalent atoms. Table 4 displays the corresponding results.

Similar to the case of Fe additions, the energy gains for Pd or Pt substitutions in Ti sites decrease, on a per atom basis, with increasing number of Pd (or Pt). Conversely, energy losses become smaller (for Pd), and gains larger (for Pt), when occupying an increasing number of Ni sites. These results indicate that, regardless of whether either one of these substitutions induce the creation of an antisite defect, Pd and Pt atoms favor Ni sites with increasing concentration for any NiTiX alloy, in spite their absolute preference for Ti sites for Ni(Ti,X) alloys. Also, in comparison with Pd, it is expected that whatever preference is displayed by Pt for Ni sites, it will be more

noticeable in both BANN and MCAS simulations than in the case of Pd.

The eight Pt atom case provides information on the role of a possible TiPt environment within the NiTi matrix. Table 6 shows the energy level spectrum of a catalog of numerous 8Pt configurations in Ni(Ti,Pt) and (Ni,Pt)Ti alloys, shown in Fig. 6. For these calculations, as we are not interested in comparing atom-by-atom energies, the optimized lattice parameters and energies and formations are shown for all possible configurations. Two opposite trends emerge: Pt(Ni) atoms tend to coalesce forming a B2 TiPt precipitate while Pt(Ti) atoms balance repulsion and attraction resulting in a '2x2' ordered pattern (where Pt(Ti) atoms are barely linked by intermediate Ti atoms in NNN positions). The only differences between the corresponding spectra for Pd and Pt consists of the energy spread between the lowest and highest energy level: 2 eV for Pd [7], and just 0.1 eV for the Pt case (and almost no change in the values of the optimized lattice parameters). There are no significant changes in the ordering of the energy levels. It should be noted that, within this model, the 'enhancement' of preference for Ni sites in Ni(Ti,X) alloys is not a direct function of X concentration, but of the ability of X atoms to create regions of higher *local* concentration.

Monte Carlo simulations provide additional information regarding the consequences of the detailed energetics described above. Fig. 7.a compares the results of BANN simulations for three different concentrations of the alloying addition X (X = Pd, Pt) in $\text{Ni}_{50-x}\text{Ti}_{50}\text{X}_x$ alloys ($x = 1, 5, 10$ at%). Not surprisingly, the absolute site preference of X for Ni sites in such alloys and the availability of sites in the Ni sublattice favor the location of Pd or Pt in Ni sites for all concentrations, with the final state being a B2 (Ni,X)Ti alloy. Fig. 7.b displays results of MCAS simulations, indicating that the thermodynamical ground state (within a rigid bcc lattice), is actually a TiX precipitate in the NiTi matrix at $T = 0$ K. At higher temperatures however, MCAS results coincide with BANN in predicting a B2 (Ni,X)Ti structure. These results are only meant to show that the ordering process is clearly related to the site preference behavior of the alloying addition, as the possibility of a martensitic transformation was not included in the simulation.

For $\text{Ni}_{(50-x/2)}\text{Ti}_{(50-x/2)}\text{X}_x$ alloys, the first sign of the competition between Ni and Ti sites can be seen. Fig. 8 shows the results of a) BANN simulations and b) MCAS simulations for $x = 2$ and 10 at%. The $\text{Ni}_{49}\text{Ti}_{49}\text{Pt}_2$ case shows a slight majority of Pt(Ni) atoms both in the 2 and 10 at% Pt: in both cases 10% of the Pt atoms go to unavailable Ni sites creating Ni(Ti) antistructure atoms, a behavior consistent with atom-by-atom analysis discussed above, where the ease with which Pt

atoms go to Ni sites was established. MCAS simulations are alike for Pd or Pt: formation of a B2 TiX precipitate for those X atoms going to Ni sites, and the formation of a ternary 2x2 phase with nearly equal number of X atoms going to Ti and Ni sites.

$\text{Ni}_{50}\text{Ti}_{(50-x)}\text{X}_x$ alloys manifest the competition between the absolute site preference for Ti sites (as displayed in Fig. 1) in contrast with the additional modeling results which indicate a trend towards Ni-site occupancy. Some representative results are shown in Fig. 9, comparing the behavior of Pd and Pt. For $\text{Ni}_{50}\text{Ti}_{49}\text{X}_1$, the BANN results (Fig. 9.a) show a stable B2 structure where 70% of the Pd atoms go to Ni sites, creating Ni(Ti) antistructure atoms. The remaining 30% perform direct substitutions for Ti sites. In the Pt case, 100% of the Pt atoms perform Ni substitutions. Once again, it is interesting to check the results of MCAS simulations at low temperatures, even if these do not include the possibility of diffusionless martensitic transformations. Fig. 9.b shows that the lowest energy state corresponds to an L2_1 Ni_2TiPd phase or, in the case of Pt, a 2x2 structure. It should be noted, however, that the difference between the L2_1 and the 2x2 structure is only in the NNN coordination and as such, it could be considered negligible.

It is important to remember that for Ni(Ti,X) alloys, within the context of these simulations, the growing energy advantage with larger Pd(Ni) or Pt(Ni) clusters still competes with the high energy cost of creating antisite Ni(Ti) defects. It is then possible that increasing Pd or Pt concentration leads to a breaking point where the energy cost of antistructure atoms inhibits the otherwise favorable X(Ni) substitutions. If the BANN simulation results, shown in Fig. 9 for $x_{\text{Pd or Pt}}=1$ and in Fig. 10 for $x_{\text{Pd or Pt}}=5$ and 10 at%, represent the statistical distribution of Pt (or Pd) atoms in Ni (or Ti) sites, then the Pt alloys show consistently a larger proportion of Pt(Ni)Ni(Ti) substitutions than in the Pd case: 90, 27, and 16% Pt(Ni)Ni(Ti) atoms for 1, 5, and 10 at% Pt concentration. For the Pd cells, there is 70, 24, and 9% Pd(Ni)Ni(Ti) atoms for 1, 5, and 10 at% Pd concentration.

c) Au, Al, Cu: As shown in Fig. 1, these elements have absolute site preference for available sites, and the energy gap with alternative configurations is too high to allow for the creation of a significant number of antistructure atoms. While this was also the case for Pd and Pt in Ni(Ti,X) alloys, the gaps are now significant for (Ni,X)Ti alloys as well. On the other hand, following the same procedure used with Pd and Pt, the formation energies of larger X(Ti) or X(Ni) clusters (regardless of whether X(Ti) or X(Ni) substitutions induce the formation of antisite defects) follow the same trends observed for Pd, as shown in Tables 2-4 and summarized in a per atom basis

in Table 5. This means that X(Ni) substitutions in (Ni,X)Ti alloys will be favored as long as other X(Ni) atoms are in the vicinity. BANN and MCAS results are shown in Fig. 4 (for $\text{Ni}_{50}\text{Ti}_{44}\text{X}_6$ alloys) and Fig. 5 (for $\text{Ni}_{44}\text{Ti}_{50}\text{X}_6$ alloys).

d) Zr, Hf: These two elements could be included in the same group as Au, Al and Cu. However, as shown in Fig. 1, there is a clear trend towards nearly equal energy gaps for substitutions in Ni or Ti sites in either (Ni,X)Ti and Ni(Ti,X) alloys strongly favoring, in either case, the available site. For these additions, the energy cost of creating antistructure defects is substantially higher than in the Au, Al and Cu cases. BANN simulations of $\text{Ni}_{50}\text{Ti}_{50-x}\text{Zr}_x$ ($x = 1, 5, 10$ at%) alloys evolve to final states with 40, 14 and 6% Zr(Ni)Ni(Ti) substitutions, while similar simulations for Hf result in 40, 7 and 6% Hf(Ni)Ni(Ti) atoms. In all cases, whether it is Hf or Zr, MCAS simulations indicate that the underlying trend is towards the substitution of Hf or Zr in Ti sites, leading to the formation of Ni_2TiX ($X = \text{Hf, Zr}$) L2_1 precipitates. The formation of this ternary phase occurs at very low temperatures (below room temperature), as the transition $\text{B2} \rightarrow \text{L2}_1$ order only involves an energy cost of approximately 0.2 eV. For $\text{Ni}_{50-x}\text{Ti}_{50}\text{Zr}_x$ ($x = 1, 5, 10$ at%) alloys, both BANN and MCAS simulations result in a small number of Zr(Ti)Ti(Ni) substitutions, where the displaced Ti(Ni) atoms tend to coalesce in a ZrTi-coated Ti precipitate (with those Zr atoms occupying Ni sites). The few Zr(Ti) atoms tend to form a Ni_2TiZr precipitate, clearly seen in MCAS simulations at low temperatures. The same is true for Hf, as shown in Fig. 5.

The results presented above compare well with the limited experimental evidence available. Nakata et al. [8-10] carried out a series of experiments to study the site occupancy of Fe, Cu, Pd and Au in NiTi. The experimental results show that Fe and Pd occupy Ni sites, irrespective of concentration. In particular, these ALCHEMI results indicate that approximately 90% of Pd goes to Ni sites for all compositions. In the case of Cu and Au, the site occupancy depends on concentration. The fractions of Pd atoms in $\text{Ni}_{49.2}\text{Ti}_{48.9}\text{Pd}_{1.9}$, $\text{Ni}_{48.4}\text{Ti}_{49.7}\text{Pd}_{1.9}$ and $\text{Ni}_{47.7}\text{Ti}_{50.3}\text{Pd}_{2.0}$ alloys were found to be 0.92, 0.94 and 0.90, respectively, indicating that Pd mostly goes to Ni sites for all compositions. The fractions of antisite Au atoms in $\text{Ni}_{49.2}\text{Ti}_{48.6}\text{Au}_{2.2}$, $\text{Ni}_{48.8}\text{Ti}_{49.1}\text{Au}_{2.1}$ and $\text{Ni}_{47.8}\text{Ti}_{50.1}\text{Au}_{2.1}$ alloys were found to be 0.14, 0.55 and 0.64, respectively, indicating that Au mostly goes to the available site. These results for Cu and Au are in agreement with the results shown in Fig. 1 and the discussion thereafter. Some indirect information on the site occupancy of Hf and Zr additions in NiTi alloys can be extracted from 3D atom probe experiments by Jung et al. [11]. Hf and Zr additions to $\text{Ni}_{53.05}\text{Ti}_{44.29}\text{Al}_{2.67}$ alloys show strong preference for Ti sites in

the Ni-rich zone. The small amount of Al suggests that probably similar results could be expected for NiTiX (X = Zr, Hf) alloys. To our knowledge, no experimental results are available for Al and Pt additions.

4. Conclusions

Modeling of the site preference behavior of X additions to NiTi benefits from extending the analysis beyond the role of one single atom X. Combining the atom-by-atom analysis with the results of different types of simulations enhances the understanding of borderline cases where the energetics of a single X atom in NiTi does not provide a complete picture of what sublattice is preferred. In this work, we implemented such procedure to determine the site preference behavior of Fe, Pt, Pd, Au, Al, Cu, Zr and Hf by means of a quantum approximate technique, the BFS method for alloys, in conjunction with large scale Monte Carlo simulations. All elements were found to prefer available sites, but a different picture emerged when other features were taken into account. Even small increments in the concentration of X in Ni(Ti,X) alloys indicate that the site preference behavior is largely driven by the XTi bonds created when X occupies Ni sites, in spite of the energy cost of creating Ni(Ti) antisite defects. This apparent loss is relieved by the low formation energy of a Ni₃Ti precipitate (although the bcc structure of this precipitate, an artifice of the simulations in rigid bcc lattices, just indicates that a Ni₃Ti ordered structure forms). BANN simulations, meant to provide an approximate picture of the evolution of the system upon cooling, support this finding, indicating (in conjunction with the atom-by-atom calculations) a trend for Ni substitutions which varies for each element.

Acknowledgements

Fruitful discussions with N. Bozzolo are gratefully acknowledged. This work was sponsored by the Alternate Energy Foundation Technologies Subproject of the Low Emissions Alternative Power Project and from the IR & D program (IRD 40-04) at the NASA Glenn Research Center, Cleveland, Ohio.

References

1. K. N. Melton, Engineering Aspects of Shape-memory Alloys, T. W. Duerig, K. N. Melton, D. Stockel and C. M. Wayman, eds., Butterworth-Heinemann, London, 1990, pp. 21-35.
2. K. Otsuka and X. Ren, *Maters. Sci. Forum* 394-395 (2002) 177.
3. K. Otsuka and X. Ren, *Intermetallics* 7 (1999) 511.
4. T. Honma, M. Matsumoto, Y. Shugo, I. Yamazaki, *ICOMAT-79: Proceedings of the International Conference on Martensitic Transformations*, Cambridge, MA, 1979, pp. 259-264.
5. R. D. Noebe, T. Biles and S. A. Padula, *Advanced Structural Materials*, W. O. Sobeyejo, Ed., Marcel Dekker, New York, 2004.
6. G. Bozzolo and J. E. Garcés, *The Chemical Physics of Solid Surfaces*, D. P. Woodruff ed., Elsevier, 2002, p. 30.
7. G. Bozzolo, R. D. Noebe and H. Mosca, *J. Alloys and Compounds* (2004) (in press).
8. T. Tadaki, Y. Nakata and K. Shimizu, *J. Phys.*, Paris, Vol. 5, C8-81 (1995).
9. Y. Nakata, T. Tadaki, K. Shimizu, *Mater. Trans. JIM* 32 (1991) 580.
10. Y. Nakata, T. Tadaki, K. Shimizu, *Mater. Trans. JIM* 32 (1991) 1120.
11. J. Jung, G. Ghosh, D. Isheim and G. Olson, *Met. Mater. Trans. A* 34 (2003) 1221.
12. H. Hosoda, A. Kamio, T. Suzuki and Y. Mishima, *J. Japan Inst. Metals* 60 (1996) 793.
13. X. D. Sheng, S. Yan, L. Dong and H. Z. Qi, *Phil. Mag. A* 75 (1997) 1185.
14. J. Smith, T. Perry, A. Banerjee, J. Ferrante and G. Bozzolo, *Phys. Rev. B* 144 (1991) 6444.
15. P. Blaha, K. Schwartz, J. Luitz, WIEN97, Vienna University of Technology. Updated Unix version of the copyrighted WIEN code, P. Blaha, P. Schwartz, P. Sorantin, S. B. Trickey, *Comput. Phys. Commun.* 59 (1990) 399.
16. G. Bozzolo, R. D. Noebe and C. Amador, *Intermetallics* 10 (2002) 149.
17. G. Bozzolo, J. Khalil and R. D. Noebe, *Comp. Mat. Sci.* 24 (2002) 457.

Table captions:

Table 1: LAPW [15] results for the lattice parameter, cohesive energy, and bulk modulus calculated for the bcc phases of Ni, Ti, Fe, Pt, Pd, Au, Al, Cu, Zr and Hf, the resulting equivalent crystal theory (ECT) [14] parameters p , α , l and λ , and the BFS perturbative parameters Δ_{AB} and Δ_{BA} .

Table 2: Difference in individual contributions to the energy of formation (in eV) of a given atom and the original (Ni or Ti) atom in the B2 cell. The gains or losses listed for the neighbor shells include every atom in that shell. Gains or losses denote changes that result in lower or higher energy of formation, respectively (see Fig. 1).

Table 3: Difference in contributions to the energy of formation (in eV) of each set of equivalent atoms and the original (Ni or Ti) atom in the B2 cell for Ni(Ti,X) alloys (X = Fe, Pt, Pd, Au, Al, Cu, Zr and Hf) with two X atoms in NNN sites. The multiplicity (M) is the number of equivalent atoms of each kind. The subindex NN (or NNN) denotes that the atom is at NN (or NNN) from the X atoms. Two types of NN are distinguished by the fact that the first 4 share both X atoms, while the other 8 are exclusively NN of only one of the X atoms. The total energy of formation of the cell is $\Delta H_{\text{NiTiX}} = \Delta H_{\text{NiTi}} + \Delta E_{\text{net}}$.

Table 4: Net gain or loss (per X atom, in eV/atom) in the energy of formation of a NiTiX alloy relative to an equilibrium NiTi B2 cell for four X atoms forming a square in a (100) plane. The multiplicity (M) is the number of equivalent atoms in the cell. The subindices denote the distance (in neighbor layers) between surrounding Ni or Ti atoms and each of the four X(Ti) (or X(Ni)) atoms, for X = Fe, Pt, Pd, Au, Al, Cu, Zr and Hf.

Table 5: Net gain or loss (per X atom, in eV/atom) in the energy of formation of a NiTiX alloy as a function of the number of X atoms (N_X).

Table 6: Energy of formation and equilibrium lattice parameter of a set of configurations with different distributions of eight Pt atoms (see Fig. 6). Arranged from higher to lower (more stable) energy, the top entries correspond to eight Pt atoms in Ti sites in a Ni(Ti,Pt) alloy. The bottom entries refer to configurations with eight Pt atoms in Ni sites in a (Ni,Pt)Ti alloy.

Figure captions:

Fig. 1: Absolute site preference behavior for X (= Fe, Pt, Pd, Au, Al, Cu, Zr, Hf) additions to (Ni,X)Ti (open squares) and Ni(Ti,X) (solid squares) alloys. Solid squares denote the energy gap γ (in eV) between X(Ti) and X(Ni)Ni(Ti) substitutions in Ni(Ti,X) alloys. Open squares denote the energy gap between X(Ni) and X(Ti)Ti(Ni) substitutions in (Ni,X)Ti alloys. Open squares high in this chart indicate that the element has a strong preference for Ni sites in (Ni,X)Ti alloys. Solid squares low in this chart indicate that the element has a very weak preference for Ti sites in Ni(Ti,X) alloys. The energy gap (in eV) is defined as the difference in energy between the lowest energy configuration (X(Ti) and X(Ni), respectively), and the average of the two states higher in energy (X(Ti)Ti(Ni)₁ and X(Ti)Ti(Ni)_f for (Ni,X)Ti, and X(Ni)Ni(Ti)₁ and X(Ni)Ni(Ti)_f for Ni(Ti,X) alloys, respectively).

Fig. 2: Changes in contributions to the energy of formation when a Fe atom occupies a Ni site. Ti atoms in NN sites to the central atom of the cluster contribute -3.4176 eV to the energy of formation of a pure NiTi cell. This contribution is changed to -3.1705 eV if the central atom in the cube shown is a Fe atom instead of the original Ni atom. For the Fe atom, the contribution of the original Ni atom in a NiTi cell is 2.7153 eV, which is lowered to 1.4656 eV when a Fe atom occupies that site. The NNN change their contribution from 2.7153 eV in a perfect B2 NiTi cell to 2.7172 eV in the presence of Fe(Ni). δE represents the gain (-) or loss (+) per atom. The total gain or loss per group of atoms is also shown. Solid (open) circles denote Ni (Ti) atoms.

Fig. 3: Energy level diagram showing the evolution of a perfect B2 NiTi cell upon (a) introduction of a Fe atom in a Ti site, and (b) insertion of the Fe atom in a Ni site, with the displaced Ni atom moving to a Ni site (see text).

Fig. 4: BANN ground state (T = 1K) and MCAS (T = 1000 K and 1 K) states for Ni₅₀Ti₄₄X₆ alloys (X = Fe, Au, Al, Cu, Zr, Hf). Ni, Ti and X atoms are denoted with grey, white and black circles, respectively.

Fig. 5: BANN ground state ($T = 1\text{K}$) and MCAS ($T = 1000\text{K}$ and 1K) states for $\text{Ni}_{44}\text{Ti}_{50}\text{X}_6$ alloys ($X = \text{Fe, Au, Al, Cu, Zr, Hf}$). Ni, Ti and X atoms are denoted with grey, white and black circles, respectively.

Fig. 6: Selected configurations with eight X atoms ($X = \text{Fe, Pt, Pd, Au, Al, Cu, Zr, Hf}$) in a B2 NiTi cell (see Table 6). Ni, Ti and X atoms are denoted with grey, white and black circles, respectively.

Fig. 7: Results of BANN and MCAS simulations for $\text{Ni}_{(50-x)}\text{Ti}_{50}\text{X}_x$ ($X = \text{Pd, Pt}$) alloys for $x = 1, 5, 10$ at%. The BANN cells show the final state for Pd (top row) and Pt (bottom row), showing a B2 (Ni,X)Ti structure. The MCAS simulations yield high and low temperature cells with X exclusively in Ni sites, forming a B2 TiX precipitate at low temperature for all concentrations.

Fig. 8: Results of (a) BANN and (b) MCAS simulations for $\text{Ni}_{(50-x/2)}\text{Ti}_{(50-x/2)}\text{X}_x$ ($X = \text{Pd, Pt}$) alloys for $x = 2$ and 10 at%.

Fig. 9: Comparison of BANN ($T = 1\text{K}$) and MCAS results for $\text{Ni}_{50}\text{Ti}_{49}\text{Pd}_1$ ($T = 1000$ and 1K) and $\text{Ni}_{50}\text{Ti}_{49}\text{Pt}_1$ ($T = 1\text{K}$) alloys. Ni, Ti and Pd (or Pt) atoms are denoted with grey, white and black circles, respectively.

Fig. 10: Final state ($T = 1\text{K}$) of BANN simulations of $\text{Ni}_{50}\text{Ti}_{(50-x)}\text{X}_x$ alloys ($X = \text{Pd, Pt}$) for two different concentrations x ($x = 5, 10$ at%). Ni, Ti and X atoms are indicated with grey, white and black circles, respectively.

Table 1
Parameters needed for performing BFS calculations of B2 NiTiX alloys.

X	Lattice parameter	Cohesive energy	Bulk modulus	ECT parameters			
	(Å)	(eV)	(GPa)	p	$\alpha(\text{Å}^{-1})$	$l(\text{Å})$	$\lambda(\text{Å})$
Ni	2.7985	5.6001	198.29	6	3.05968	0.29494	0.82878
Ti	3.2552	5.7825	105.44	6	2.69236	0.38109	1.07085
Fe	2.7565	4.7421	277.60	6	2.98304	0.23112	0.64946
Pt	3.1630	5.6268	237.76	10	4.32439	0.25396	0.71362
Pd	3.1358	4.0148	172.45	8	3.48602	0.25297	0.71086
Au	3.3132	3.1497	134.87	10	4.07890	0.24649	0.69264
Al	3.2400	3.4226	69.38	4	1.76092	0.36229	1.01803
Cu	2.8957	3.6722	150.97	6	2.88785	0.26907	0.75613
Zr	3.5765	6.2559	87.09	8	3.28559	0.41610	1.16924
Hf	3.5507	6.8319	100.76	10	4.13573	0.40572	1.14007

BFS parameters (in Å ⁻¹)				
X	Δ_{NiX}	Δ_{XNi}	Δ_{TiX}	Δ_{XTi}
Ni	0	0	0.481946	-0.074001
Ti	-0.074001	0.481946	0	0
Fe	-0.019382	0.054565	0.152825	-0.066734
Pt	-0.031262	-0.044047	0.102297	-0.072062
Pd	-0.021765	-0.037241	0.080218	-0.064662
Au	-0.037401	0.061145	0.100375	-0.064929
Al	-0.040894	0.039742	0.081892	-0.063261
Cu	-0.042889	0.134320	0.085030	-0.052742
Zr	-0.083302	0.155333	0.127582	-0.063102
Hf	-0.101624	0.173086	0.115974	-0.058777

Table 2

Net changes in the contributions to the energy of formation due to the substitution of a single X atom in NiTi alloys. ΔE_{net} denotes the net energy gain (-) or loss (+) with respect to a NiTi cell.

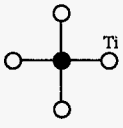
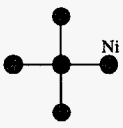
Alloy	Atom	Fe	Pt	Pd	Au	Al	Cu	Zr	Hf
Ni(Ti,X)	X(Ti)	+3.8254	+3.2351	+3.3390	+3.0953	+2.2700	+2.8120	+1.9519	+1.5120
	(8x)Ni _{NN}	-2.4296	-3.4450	-3.3669	-2.3696	-2.5668	-1.7672	-1.6132	-1.4890
	(6x)Ti _{NNN}	-0.5466	-0.5973	-0.5280	-0.5298	-0.5150	-0.4200	-0.5135	-0.4741
	ΔE_{net}	+0.8492	-0.8072	-0.5558	+0.1959	-0.8118	+0.6248	-0.1748	-0.4511
(Ni,X)Ti	X(Ni)	-1.2497	-1.2489	-1.8161	-0.7362	-1.7404	-2.2071	+0.8370	+0.4972
	(8x)Ti _{NN}	+1.9768	+0.5546	+2.4940	+2.4288	+2.8327	+5.1448	+2.8707	+3.8658
	(6x)Ni _{NNN}	+0.0114	-0.1087	+0.0091	+0.0132	+0.0087	+0.0258	+0.0292	+0.0318
	ΔE_{net}	+0.7385	-0.7052	+0.6688	+1.7058	+1.1010	+2.9635	+3.7369	+4.3948

Table 3
Atom-by-atom energetics of two X atoms in NiTi

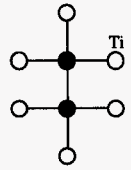
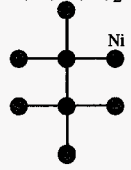
Configura- tion	M	Ni(Ti,X)	Fe	Pt	Pd	Au	Al	Cu	Zr	Hf
	2	X(Ti)	+7.6456	+6.4630	+6.6738	+6.1762	+4.4490	+5.6042	+3.7724	+2.9302
	4	Ni _{NN}	-2.4268	-3.4356	-3.3584	-2.3676	-2.5640	-1.7668	-1.6128	-1.4888
	8	Ni _{NN}	-2.4296	-3.4448	-3.3672	-2.3696	-2.5672	-1.7692	-1.6136	-1.4888
	10	Ti _{NNN}	-0.9110	-0.9950	-0.8790	-0.8830	-0.8580	-0.7000	-0.8550	-0.7900
			ΔE_{net}	+1.8782	-1.4124	-0.9308	+0.5560	-1.5402	+1.3682	-0.3090
	2	X(Ni)	-2.4988	-2.4964	-3.6314	-1.4712	-3.4742	-4.4124	+1.6938	+1.0112
	4	Ti _{NN}	+1.8732	+0.5460	+2.3328	+2.2752	+2.6284	+4.5332	+2.6612	+3.5024
	8	Ti _{NN}	+1.9768	+0.5552	+2.4944	+2.4288	+2.8328	+5.1448	+2.8712	+3.8664
	10	Ni _{NNN}	+0.0190	-0.0180	-0.0150	+0.0220	+0.0140	+0.0430	+0.0480	+0.0530
			ΔE_{net}	+1.3702	-1.4132	+1.1808	+3.2548	+2.0010	+5.3086	+7.2742

Table 4
Atom-by-atom energy analysis of four Pd atoms in NiTi

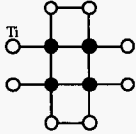
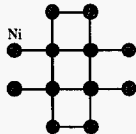
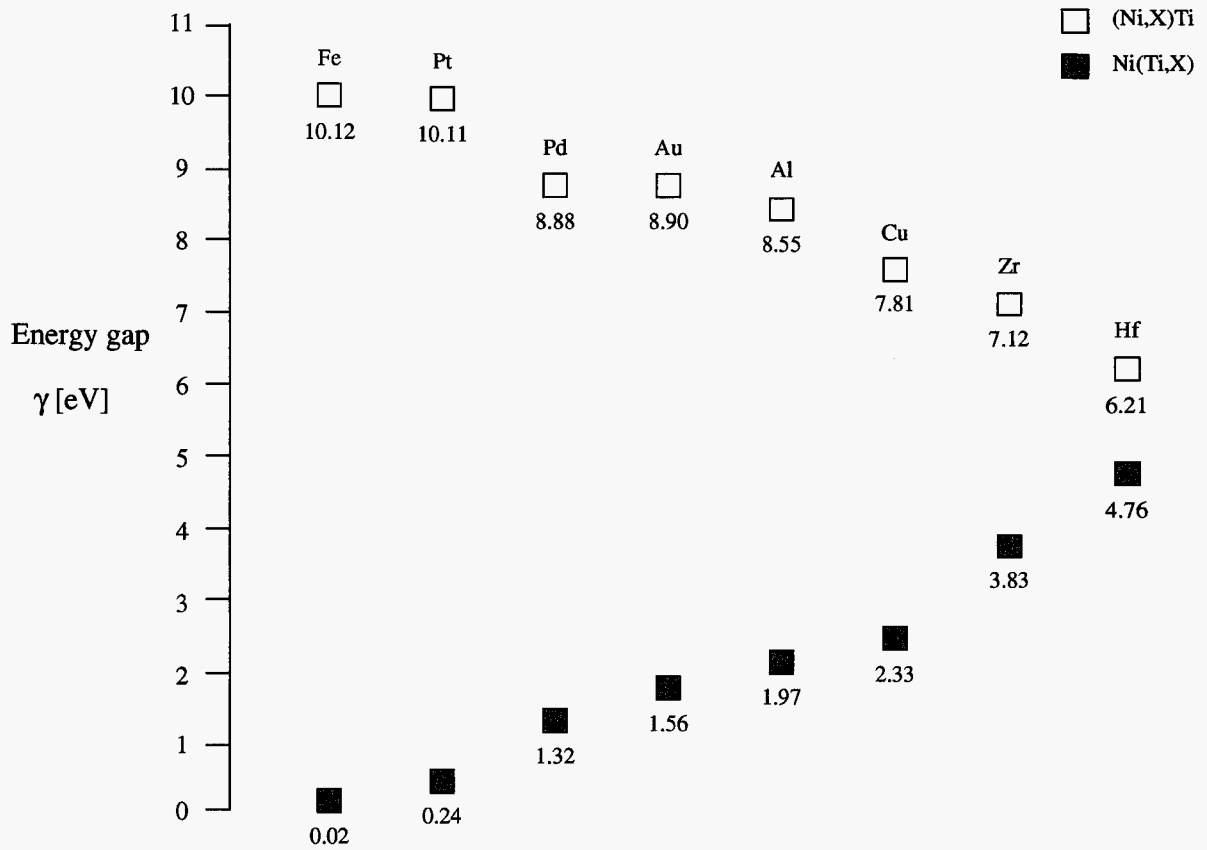
Configu- ration	M		Fe	Pt	Pd	Au	Al	Cu	Zr	Hf	
	Ni(Ti,X)	4	X(Ti)	+15.2812	+12.9108	+13.3392	+12.3236	+8.7084	+11.1676	+7.2756	+5.6696
		2	Ni _{NN}	-2.4082	-3.3580	-3.2878	-2.3504	-2.5406	-1.7616	-1.6092	-1.4862
		8	Ni _{NN}	-4.8536	-6.8712	-6.7168	-4.7352	-5.1280	-3.5336	-3.2256	-2.9776
		8	Ni _{NN}	-2.4296	-3.4448	-3.3672	-2.3696	-2.5672	-1.7621	-1.6136	-1.4888
		16	Ti _{NNN}	-1.4576	-1.5920	-1.4064	-1.4128	-1.3728	-1.1200	-1.3680	-1.2640
			ΔE_{net}	+4.1322	-2.3552	-1.4390	+1.4556	-2.9002	+2.9852	-0.5408	-1.5470
	(Ni,X)Ti	4	X(Ni)	-4.9964	-4.9896	-7.2612	-3.3580	-6.9348	-8.8208	+3.4272	+2.0564
		2	Ti _{NN}	+1.7014	+0.5292	+2.0766	+2.0410	+2.3106	+3.7010	+2.3362	+2.9724
		8	Ti _{NN}	+3.7464	+1.0920	+4.6656	+4.6480	+5.2568	+9.0664	+5.3224	+7.0048
		8	Ti _{NN}	+1.9768	+0.5552	+2.4944	+2.5584	+2.8328	+5.1448	+2.8712	+3.8664
		16	Ni _{NNN}	+0.0304	-0.0288	-0.0240	-0.2720	+0.0224	+0.0688	+0.0768	+0.0848
			ΔE_{net}	+2.4586	-2.8420	+1.9514	+5.6174	+3.4878	+9.1602	+14.0338	+15.9848

Table 5
Net gain or loss (per X atom) in the energy of formation of a NiTiX alloy
relative to B2 NiTi as a function of number of X atoms

Alloy	N_X	Fe	Pt	Pd	Au	Al	Cu	Zr	Hf
Ni(Ti,X)	1	+0.8492	-0.8072	-0.8072	+0.1959	-0.8118	+0.6248	-0.1748	-0.4511
	2	+0.9391	-0.7062	-0.7062	+0.2780	-0.7701	+0.6841	-0.1545	-0.4187
	4	+1.0330	-0.5888	-0.5888	+0.3639	-0.7250	+0.7463	-0.1352	-0.3867
(Ni,X)Ti	1	+0.7385	-0.7052	-0.7052	+1.7058	+1.1010	+2.9635	+3.7369	+4.3948
	2	+0.6851	-0.7066	-0.7066	+1.6274	+1.0005	2.6543	+3.6371	+4.2165
	4	+0.6146	-0.7105	-0.7105	+1.4043	+0.8719	2.2900	+3.5084	+3.9962

Table 6
Energies of formation of different eight Pt atoms configurations in NiTi

Configuration	Energy of formation (eV)	Lattice parameter (Å)	Configuration
Eight Pt(Ti) atoms in a Ni(Ti,Pt) cell	-0.35672	3.01846	(a) Eight isolated Pt(Ni) atoms in different planes
	-0.35673	3.01846	(g) Four Pt(Ni) coplanar dimers
	-0.35674	3.01846	(f) Two 4Pt(Ni) chains separated by a Ni row
	-0.35675	3.01846	(e) Eight Pt(Ni) chain
	-0.35678	3.01845	(c) Rectangular Pt(Ni) patch (4 consecutive dimers)
	-0.35678	3.01845	(d) Hexagonal 8Pt(Ni) patch
	-0.35681	3.01845	(b) B2 Pt(Ni)Ti precipitate
Eight Pt(Ni) atoms in a (Ni,Pt)Ti cell	-0.35314	3.01315	(a) Eight isolated Pt(Ti) atoms in different planes
	-0.35430	3.01441	(b) B2 NiPt(Ti) precipitate
	-0.35431	3.01429	(c) Rectangular 8Pt(Ti) patch (4 consecutive dimers)
	-0.35550	3.01427	(d) Hexagonal 8Pt(Ti) patch
	-0.35587	3.01422	(e) Eight Pt(Ti) chain
	-0.35629	3.01418	(f) Two 4Pt(Ti) chains separated by a Ti row
	-0.35666	3.01414	(g) Four Pt(Ti) coplanar dimers
	-0.35751	3.01406	(h) 2x2 patch



Alloy	Atom	Fe	Pt	Pd	Au	Al	Cu	Zr	Hf
(Ni,X)Ti	X(Ni)	-0.2611	-1.7052	-0.3316	0.7050	0.1010	1.9632	2.7370	3.3948
	X(Ti)Ti(Ni) ₁	9.3193	8.0670	8.1058	9.4510	8.5626	9.3748	10.3418	10.1104
	X(Ti)Ti(Ni) _f	10.4041	8.7478	8.9992	9.7505	8.7432	10.1794	9.3802	9.1039
	γ	10.1228	10.1126	8.8841	8.8957	8.5519	7.8139	7.1240	6.2123
Ni(Ti,X)	X(Ti)	-0.1510	-1.8072	-1.5558	-0.8045	-1.8118	-0.3756	-1.1748	-1.4511
	X(Ni)Ni(Ti) ₁	-0.1269	-1.5593	-0.2811	0.6730	0.0834	1.8153	2.4423	3.0846
	X(Ni)Ni(Ti) _f	-0.1287	-1.5727	-0.1991	0.8375	0.2335	2.0957	2.8694	3.5273
	γ	0.02318	0.2412	1.3157	1.5598	1.9703	2.3311	3.8307	4.7571

Fig. 1

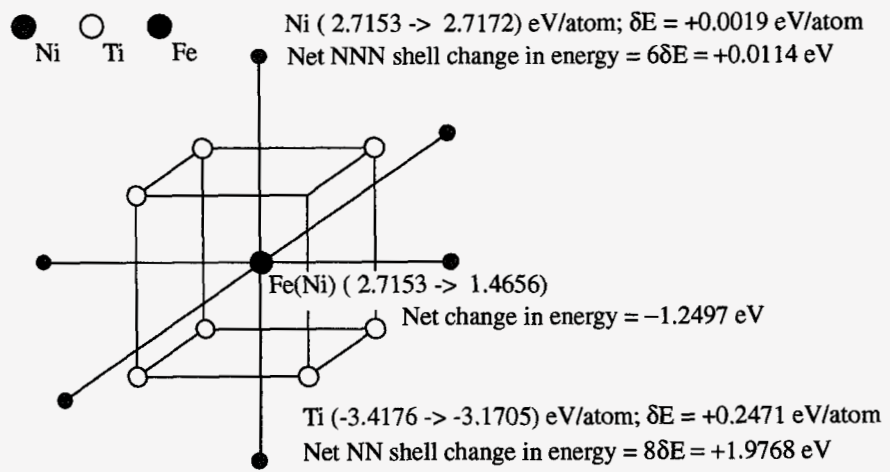


Fig. 2

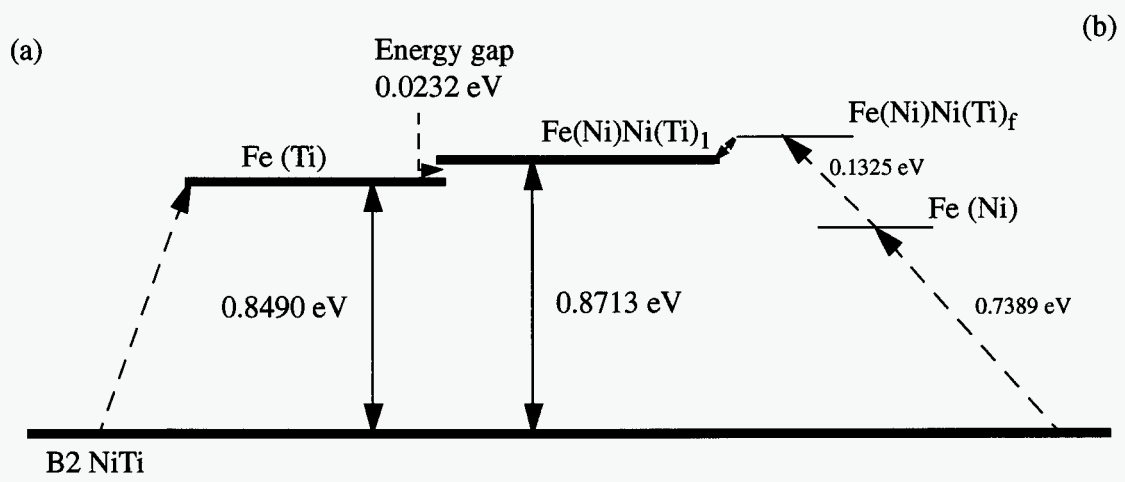


Fig. 3

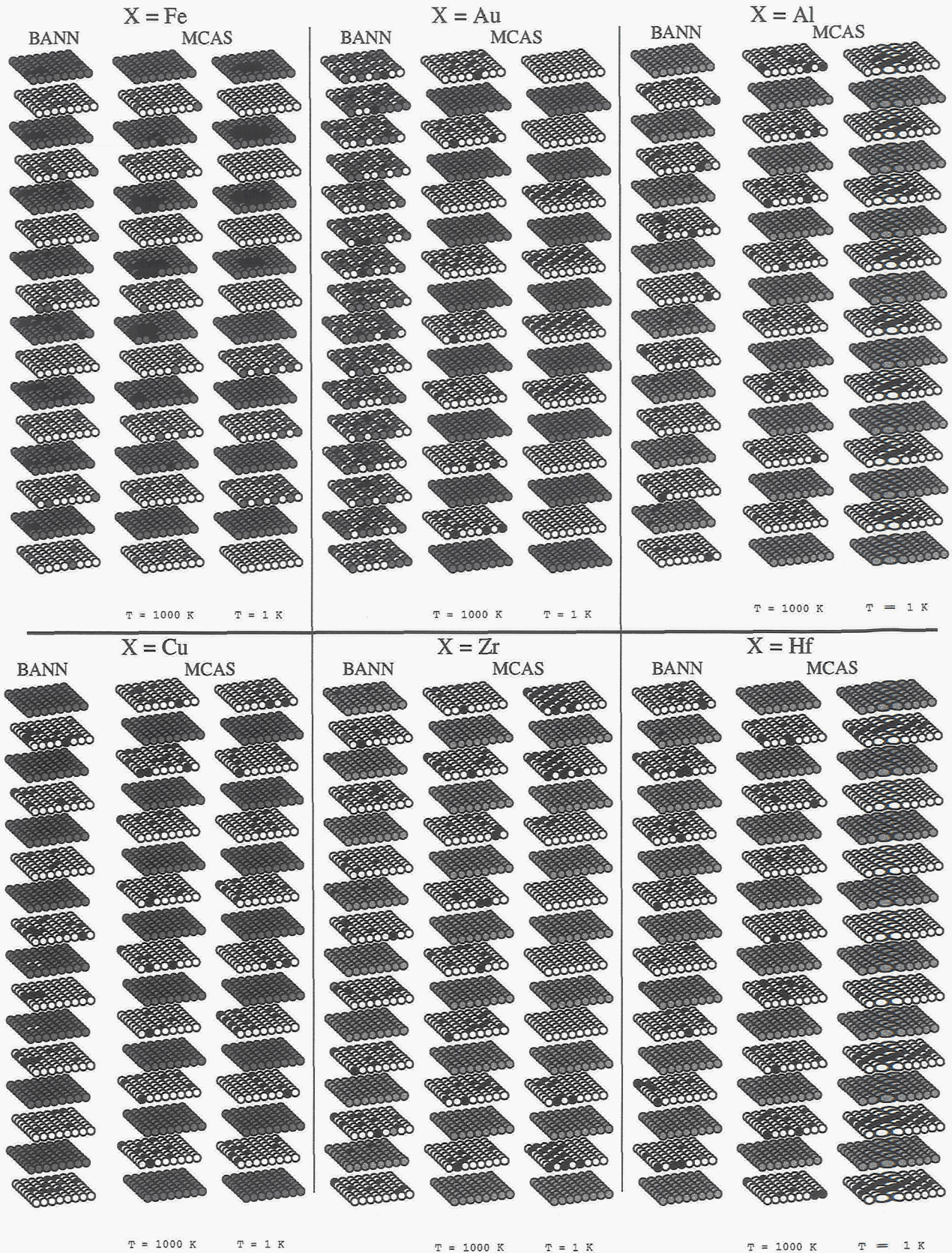
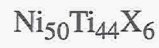


Fig. 4

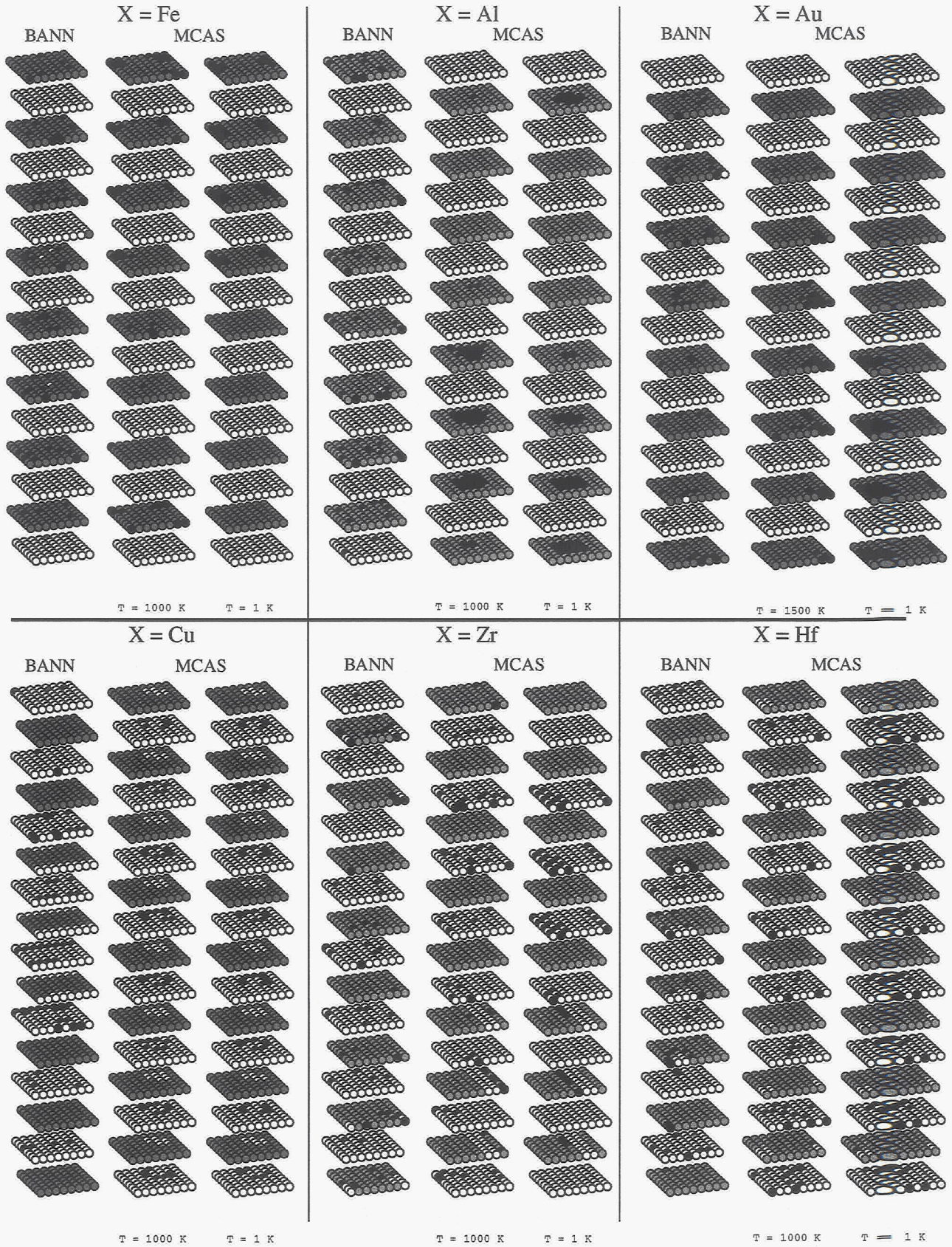


Fig. 5

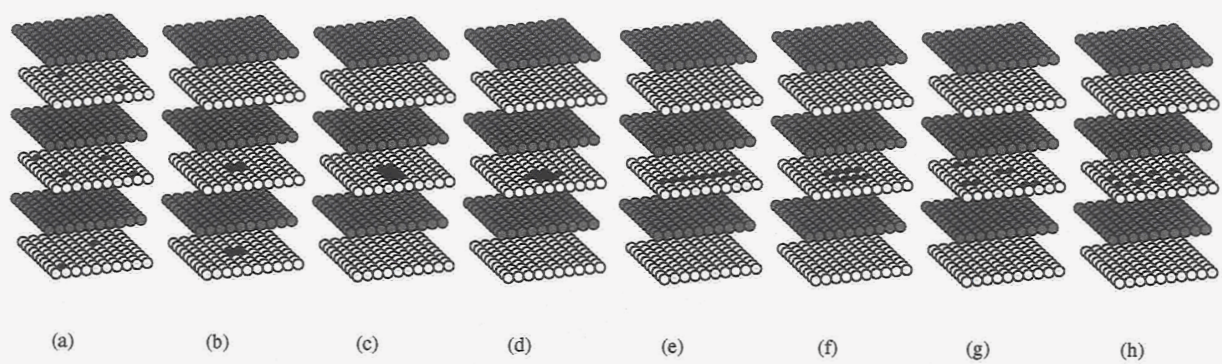


Fig. 6

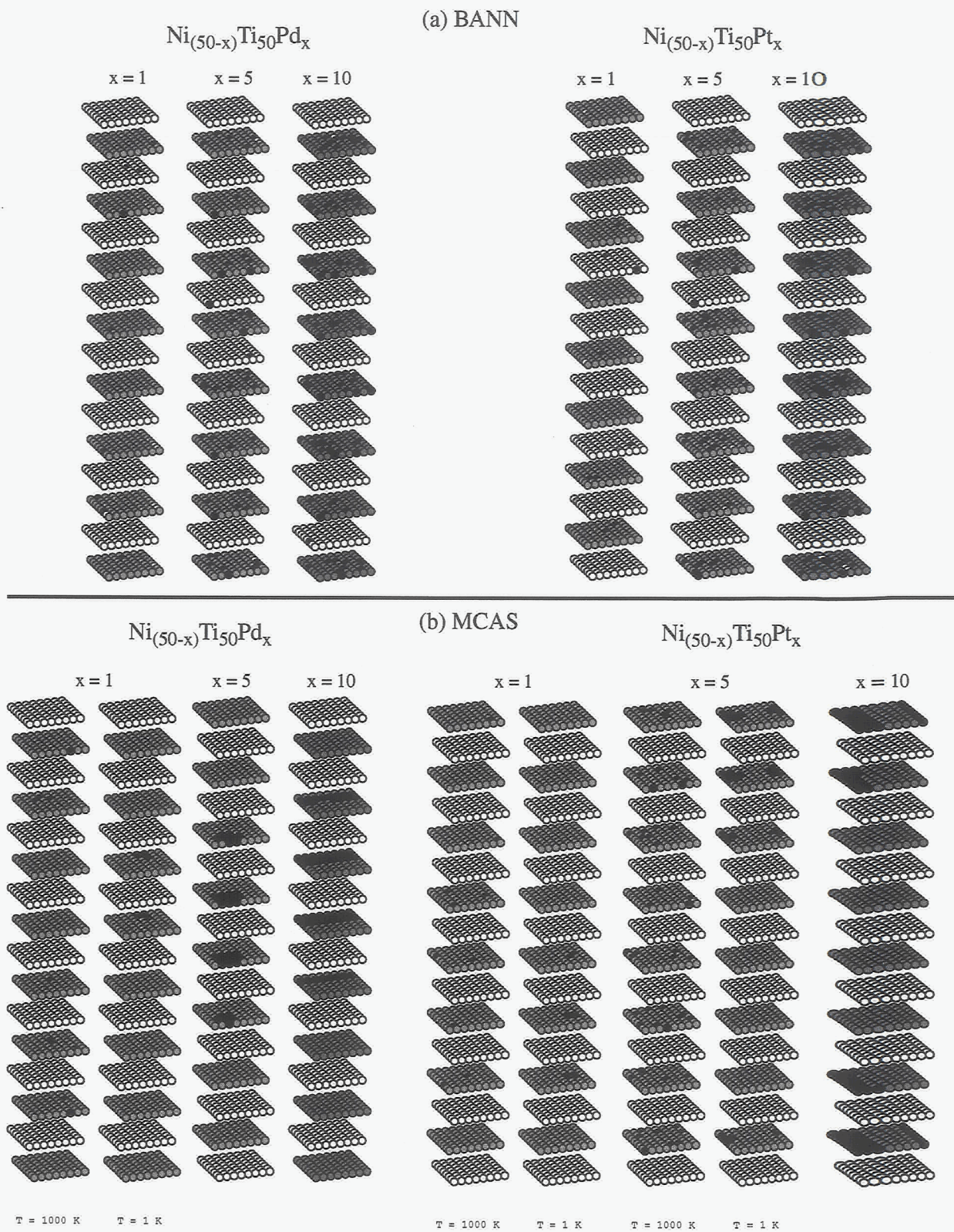


Fig. 7

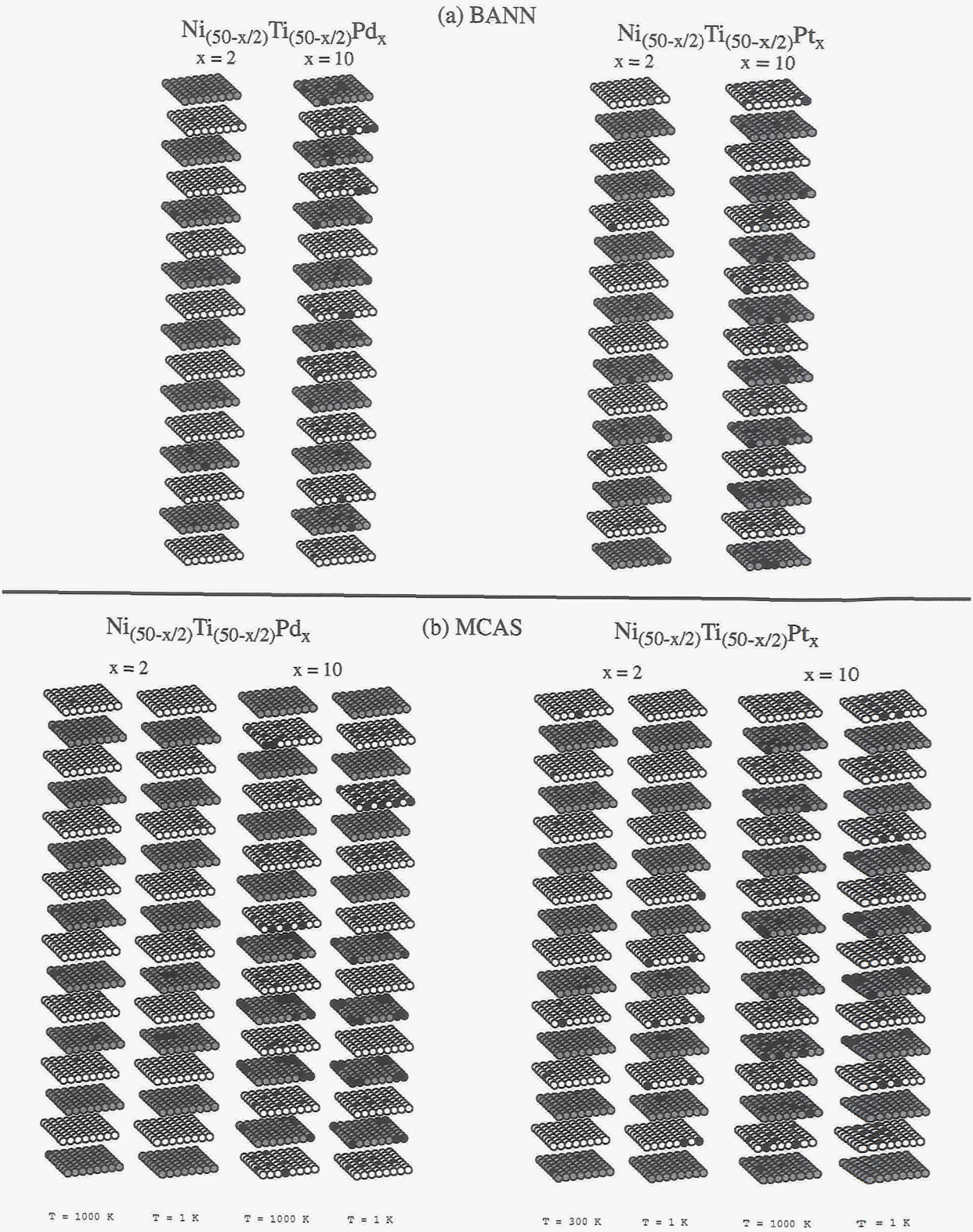


Fig. 8

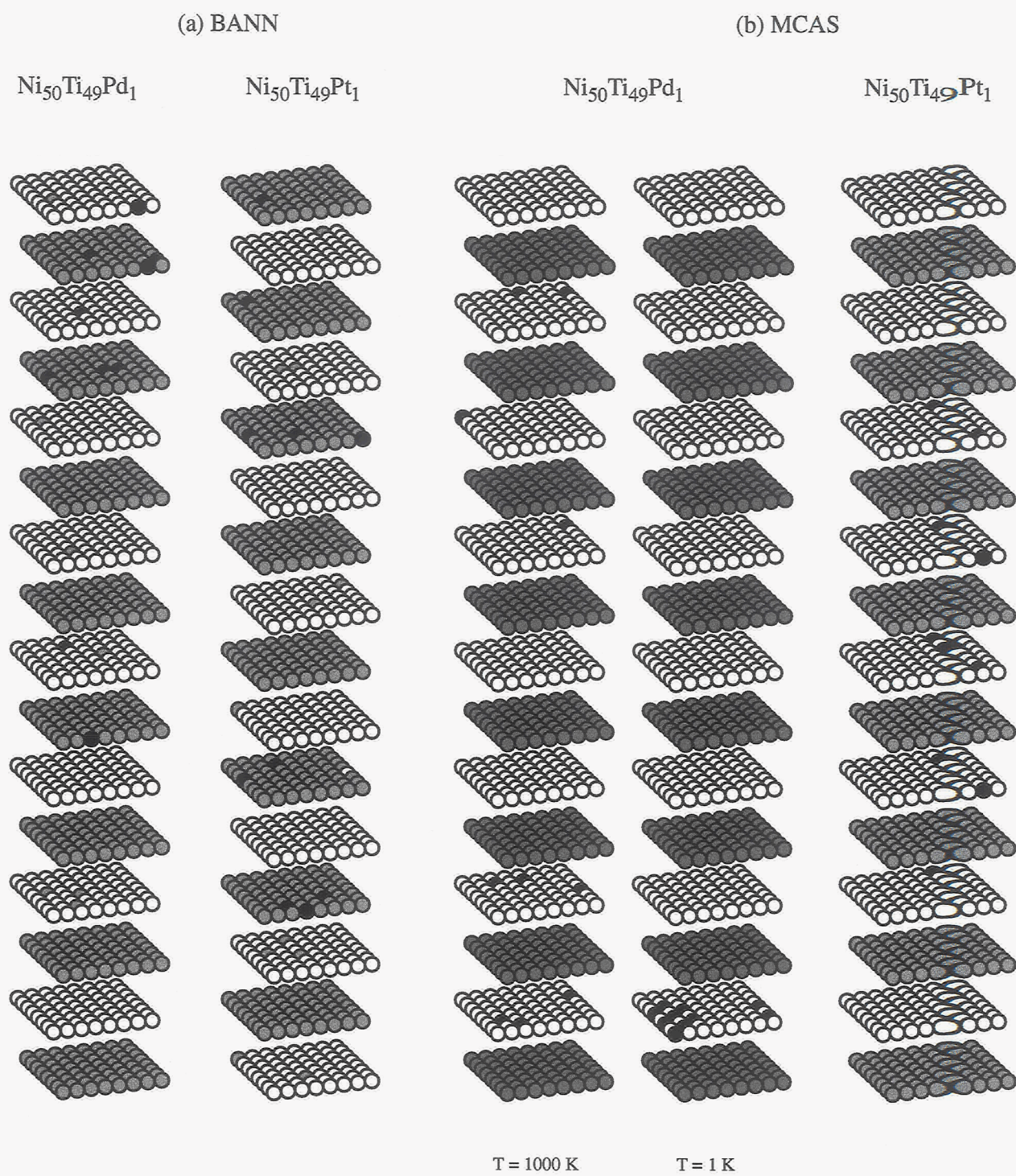


Fig. 9

(a) $X_{Pd/Pt} = 5 \text{ at}\%$

(a) $X_{Pd/Pt} = 10 \text{ at}\%$

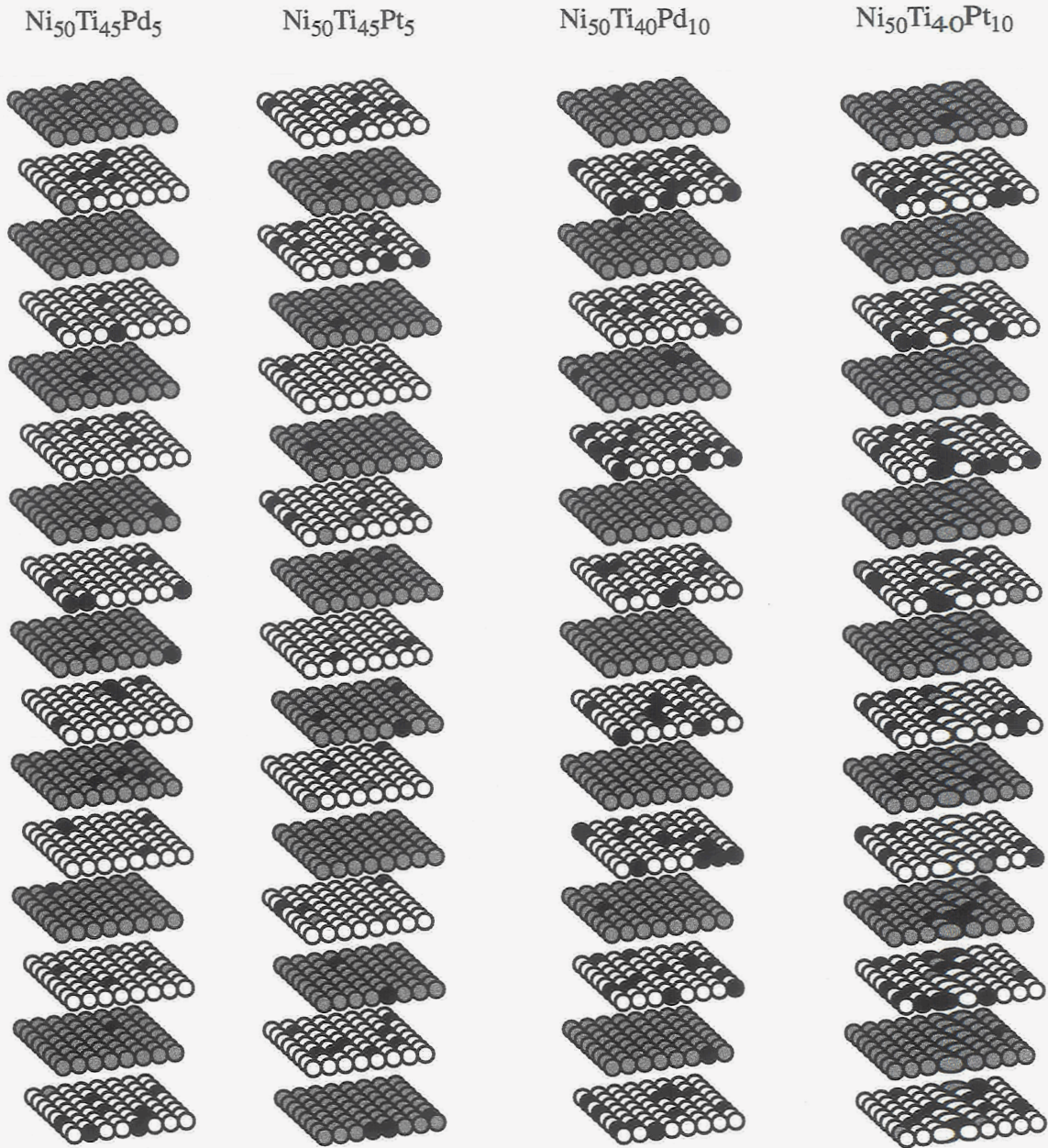


Fig. 10